

See discussions, stats, and author profiles for this publication at: <https://www.researchgate.net/publication/277887067>

A New Class of Nitroanilinic Dimer, the PNA O-Dimer: Electronic Structure and Emission Characteristics of O-Dimeric Aggregates

ARTICLE *in* THE JOURNAL OF PHYSICAL CHEMISTRY A · JUNE 2015

Impact Factor: 2.69 · DOI: 10.1021/acs.jpca.5b03645

READS

21

1 AUTHOR:



Nikhil Aggarwal

Indian Institute of Technology Madras

3 PUBLICATIONS 0 CITATIONS

[SEE PROFILE](#)

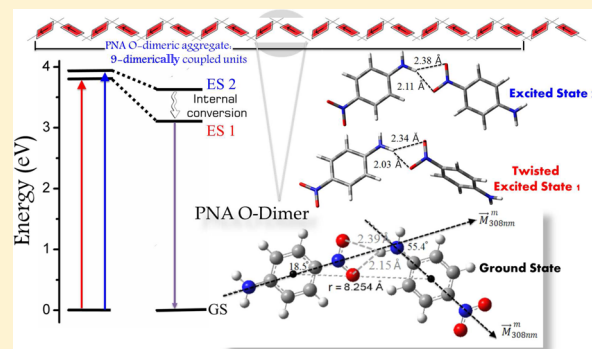
A New Class of Nitroanilinic Dimer, the PNA O–Dimer: Electronic Structure and Emission Characteristics of O–Dimeric Aggregates

Nikhil Aggarwal and Archita Patnaik*

Colloid and Interface Chemistry Laboratory, Department of Chemistry, Indian Institute of Technology Madras, Chennai 600036, India

S Supporting Information

ABSTRACT: *p*-Nitroaniline (PNA) has been reported as a “J” aggregate species. In retrospect, this communication confirms a radically different “oblique” orientation of the PNA units in all three solid, liquid, and gas phases of the dimer, the O-dimer. The nonvanishing transition dipole moments (TDM) associated with the allowed electronic excitations of the O-dimer, computed using electron–hole pair density distribution (EDD and HDD) analyses ascertained the two monomers to be inclined at slippage (θ) and polarization (α) angles of 18.5° and 55.4° , respectively. A detailed structure–property relationship of the PNA O-dimeric aggregate was carried out using UV–vis absorption and matrix scan emission spectroscopy, supported by electronic structure calculations at DFT-M062X/6-31G+(d,p) level using integral equation formalism polarizable continuum model (IEPCM). The computed potential energy surface (PES) implied the global minimum of the PNA O-dimer stabilized by $4.8 \text{ kcal.mol}^{-1}$, owing to bifurcated intermolecular hydrogen bonding. In the excited PNA O-dimeric aggregate, an exchange of excitation energy between the monomeric units resulted in two distinct electronic states separated by an interaction energy of -1644 cm^{-1} . The TD-DFT computed excited state equilibrium structures of the PNA O-dimer corroborated the experimentally observed pronounced Stoke’s shift to internal conversion following vibrational relaxation of the allowed electronic excited states. On the basis of the detailed structural analysis of PNA O-dimer, the observed energy shifts in optical absorption spectroscopy were evident within the framework of exciton coupling model.



INTRODUCTION

Low-dimensional organic supramolecular structures such as conjugated polymers, natural pigment–protein complexes, or dendrimers have attracted considerable interest in recent years. Features such as fast and efficient energy transfer, nonlinear optical behavior, and tunability of optical properties make molecular aggregates promising candidates for the development of new optoelectronic devices with tailored properties. Optoelectronically active molecular aggregates are classified into J- and H-type on the basis of characteristic slippage angle (θ), defined as the angle subtended by the line joining centers of two monomeric units and the polarization axis. Although $\theta \leq 54.7^\circ$ in J-dimers and $\theta \geq 54.7^\circ$ in H-dimers are validated,¹ the transition dipole moment’s (TDM) direction corresponding to monomeric electronic excitation has shown a parallel orientation of monomers in both types of molecular dimers, depicted in Figure 1a,b. The intriguing optical properties of J-aggregates, in particular, very narrow red-shifted absorption bands with respect to those of the monomer and their ability to delocalize and migrate an exciton, were evident for cyanine,^{2,3} perylene bisimide,^{4,5} merocyanine,⁶ and azobenzene^{7–9} families. Moreover, J-aggregates are highly fluorescent; in contrast, rapid internal conversion of the allowed higher energy exciton state to the forbidden lower energy exciton state quenches the

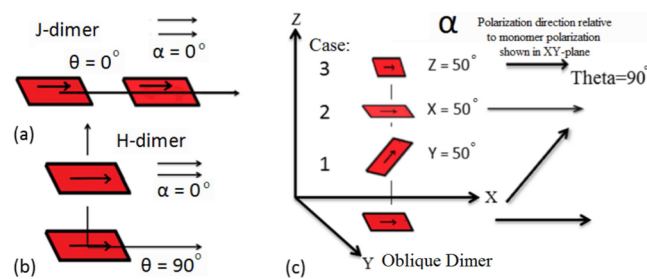


Figure 1. (a), (b) monomer arrangements in H and J dimers with the arrows representing the transition dipole moment direction. α and θ represent the polarization and slippage angles, respectively. (c) Scheme drawn to show the monomeric arrangement in three different O-dimers, where monomers are aligned by rotation along x , y , and z axes with a polarization angle of 50° with respect to the monomer shown in the XY plane.

fluorescence in H-aggregates.¹⁰ This behavior was already observed for a large number of dimeric aggregates of classical fluorophores, including fluorescein,¹¹ eosin, thionine, methyl-

Received: April 16, 2015

Revised: June 7, 2015



ACS Publications

© XXXX American Chemical Society

A

DOI: 10.1021/acs.jpca.5b03645
J. Phys. Chem. A XXXX, XXX, XXX–XXX

ene blue, and certain cyanine dyes, and the nonemissive character of the excited state became commonly accepted as a general feature of H-aggregates.^{12,13}

H-aggregate arrangements with considerable $\pi-\pi$ overlap were considered detrimental for light amplification. However, unexpected merocyanine H-aggregates exhibiting substantial fluorescence with significantly longer fluorescence lifetime were reported.¹⁴ On the basis of small transition probability to a forbidden exciton state caused by a meager rotation of one of the coupled dyes in the ground state, the observed fluorescence was rationalized within the exciton theory. On a similar note, *p*-distyrylbenzene formed highly luminescent H-aggregates¹⁵ in single crystals in view of low trap concentration but became feebly emissive in polycrystalline nanoparticle suspensions and vapor-deposited or spin-coated films. Varghese et al.¹⁶ observed stimulated emission from cofacially arranged distyrylbenzenes upon minimization of $\pi-\pi$ overlap between the adjacent fragments. These basic and easily recognizable bathochromic and hypsochromic spectral changes relative to monomer absorption have indicated molecular properties of the building blocks to be significantly altered upon aggregation.

Although H- and J-dimers represent ideal cases of molecular dimers, the intermediate angular orientations of the dipoles result in the oblique structure. Here, the transition dipoles may or may not be parallel to each other with variation in the slippage angle between 0 and 90°, depicted in Figure 1c. Accordingly, the polarization angle (α), defined as the angle subtended by the polarization axes between monomers, is a more suitable choice to define the oblique structure of molecular dimers. In Figure 1c, three different O-dimeric structures are schematically depicted corresponding to 50° polarization angle with respect to the monomeric unit in the XY-plane. Forster's coupled oscillator model¹⁷ and Kasha's exciton splitting model¹ have theoretically interpreted the optical properties of O-dimeric aggregates. Accordingly, for the majority of possible dimeric structures, the exchange of excitation energy between monomeric units splits an exciton band into two absorption bands, one at a higher ("H-band") and the other at a lower ("J-band") energy with reference to the monomeric absorption band. Thus, for the perfect H- and J-aggregates, transition to out-of-phase arranged dipoles is fully forbidden (Figure S1, Supporting Information). In retrospect, for an O-dimer, a finite value of polarization angle leads to nonvanishing transition dipole moments for both electronic transitions. Consequently, the spectral signatures for an O-dimer differ from both H- and J-dimers with red- and blue-shifted absorption features. Despite this fact, the dye aggregates have been most commonly classified as H- and J-type on the basis of their most intense absorption bands.

Conjugated organic materials based on D- π -A structure (a π conjugated backbone bridging donor and acceptor groups) have been intensively studied during the last decades for application in optoelectronic devices.^{18,19} Although the majority of the materials were based on polymers due to their easy processability, there is a clear tendency in recent years toward small molecules; in fact, the latest recorded values for efficiencies of optical solar cells are based on small molecule devices.^{20–23} Moreover, the possibility to better control the intermolecular arrangement compared to the polymeric materials was demonstrated to be beneficial.^{24,25} Also, well-defined oligomeric molecules with clever design of molecular backbone and substituent pattern could drive the molecules into specific intermolecular arrangements, controlled through

secondary forces such as local dipoles and hydrogen bonds.²⁴ This is especially true for the nanoalignment at interfaces needed for optoelectronic functionality.

Nitroanilines due to large second-order microscopic polarizabilities²⁶ are good candidates for nonlinear optical (NLO) materials.^{27,28} However, many nitroanilines do not exhibit second harmonic generation (SHG) in the solid state as they pack into the centrosymmetric crystal structure.^{29,30} In a very detailed work by Etter and co-workers, it was shown that hydrogen bond interaction plays an important role in the packing patterns of nitroanilines.^{31,32} Moreover, Yuan-Hang et al.³³ have theoretically demonstrated aggregation effects on two-photon absorption cross sections of di-, tri-, and tetrameric *p*-nitroaniline (PNA) and compared the results with results for individual PNA molecules from the hydrogen bond interaction. Despite intense computational investigations on various nitroanilinic systems,^{34–38} photophysical processes of nitroaniline functionalized molecular dimers are still not completely captured. *p*-Nitroaniline is known to possess large NLO response and represents a prototype example of a donor- π -acceptor system. In contrast to the commonly reported PNA J-dimeric aggregates, the present investigation confirms the "oblique" orientation of the PNA dimer formed via bifurcated H-bonding from the experimental and computed ground and excited state equilibrium structures. Consequently, the angle between the monomeric TDMs was estimated and the excitonic behavior in the oblique geometry was explained in accordance with the molecular exciton model.

METHODS

i. Computational Details. *a. Ground and Excited State PNA Monomer and Dimer Geometries.* The ground state structure of the PNA monomer and the dimer were computed with DFT-B3LYP/6-31G+(d,p) and DFT-M062X/6-31G+(d,p) levels of theory, respectively. Bulk solvent effects have been taken into account using the integral equation formalism polarized continuum model (IEPCM) with DFT and TD-DFT methods for geometry optimization and allowed electronic transitions, respectively, following the Gaussian 09 program package.³⁹ The polarization continuum model (PCM) offers the undeniable advantage of correctly describing average polarization of the environment and its effect on the chromophore without any explicit sampling of solvent coordinates. The functional used was selected on the basis of previous benchmarks.^{40–42} M062X⁴³ as the hybrid meta-exchange-correlation functional was used for specifically incorporating the H-bonded interactions. All optimizations were performed with tight convergence criteria without any symmetry constraints, followed by frequency calculations to ensure the global minima of the stationary points. The theoretical determination of excited state structures remains an active field of research, as these data are hardly accessible by experimental approaches. In this contribution, equilibrium structures of the PNA dimeric excited states along with the emission characteristics were unraveled following the TD-DFT-M062X/6-31G+(d,p) method with IEFPCM. Because inferring on the aggregate geometry via large scale computation was cumbersome,^{44,45} the representative O-dimer geometry predicted the behavior of the O-dimeric aggregates. Figure S1 (Supporting Information) depicts the exciton splitting energy for the ideal dimeric systems.

b. Electron and Hole Density Distribution (EDD and HDD) Profiles for the Excited States of PNA Monomer and O-

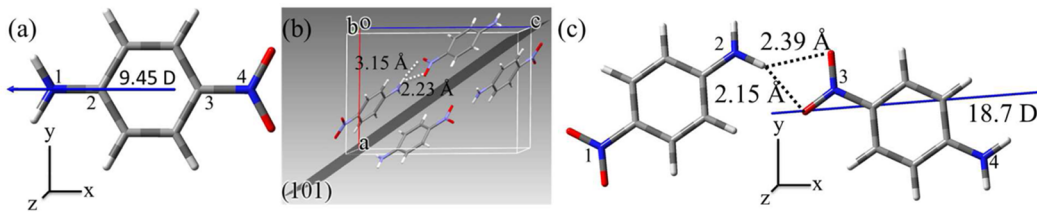


Figure 2. (a) Computed structure of the planar PNA monomer showing the direction of dipole moment. (b) Single crystal unit cell structure of PNA (see ref 48). (c) Ground state optimized structure of the PNA dimer in THF along with its dipole moment computed at DFT-M062X/6-31G+(d,p) level with IEFPCM showing bifurcated H-bonding.

Dimer. Electron ($\rho^{\text{ele}}(r)$) and hole ($\rho^{\text{hole}}(r)$) density distribution maps are characteristic regions belonging to photoexcited states with similarity to ground state molecular orbitals. Lu and Chen^{46,47} have shown the EDD and HDD to be described in terms of molecular orbital wave function (Φ) and configuration coefficient (w) corresponding to transition of an electron from occupied MO(i) to a virtual MO(l) on electronic excitation, vide eqs 1 and 2.

$$\rho^{\text{ele}}(r) = \sum_{i \rightarrow l} (w_i^l)^2 \Phi_l(r) \Phi_i(r) + \sum_{i \rightarrow l} \sum_{i \rightarrow m \neq l} w_i^l w_m^m \Phi_l(r) \Phi_m(r) \quad (1)$$

$$\rho^{\text{hole}}(r) = \sum_{i \rightarrow l} (w_i^l)^2 \Phi_l(r) \Phi_i(r) + \sum_{i \rightarrow l} \sum_{j \neq i} w_i^l w_j^j \Phi_l(r) \Phi_j(r) \quad (2)$$

The above formalism was used in the present investigation for computing EDD and HDD maps for the PNA monomer and the dimer. Calculations were performed at the DFT-M062X/6-31G+(d,p) level with IEFPCM in THF using Multiwfn 3.3.4 developed by Lu.^{46,47} The direction of TDM was defined as the line joining the centroids of EDD and HDD maps for the associated electronic transitions.

ii. Experimental Details. UV-vis absorption spectra and steady state matrix scan emission spectra of PNA in tetrahydrofuran (THF) at varying concentrations were acquired using JASCO V-650 spectrophotometer and JASCO FP-6300 spectrofluorometer at room temperature.

RESULTS AND DISCUSSION

Equilibrium Geometry and Energetics of the PNA Dimer: Validating the O-Dimer Structure. Despite numerous theoretical efforts,^{34–38} the definitive structure of PNA dimer is still debatable. Two PNA dimer conformations have accounted for the global minimum: the face-to-face stacked H-dimeric structure and the head-to-tail packed J-dimeric structure, where preference for the latter was supported from the theoretically computed PNA dimeric structure at HF/6-31G**³⁶ and MP2/6-31G+(d,p) levels of calculation.³⁴ In addition, existence of the face-to-face stacked PNA H-dimeric structure was suggested from the nonlinear optical response of its charged centrosymmetric aggregates using ab initio supermolecular approach.³⁷ Therefore, the need for structure elucidation of the PNA dimer is more than topical and warrants unambiguous experimental and computational data.

The computationally obtained ground state optimized structure of the archetypal chromophore PNA monomer in THF (cf. Figure 2a) shows N₁–C₂–C₃–N₄ dihedral angle between the central benzene ring and the –NO₂ and –NH₂ fragments as 179°, validating the planarity of the monomer. The equilibrium structure could be thought of as supporting an H-dimer formation via π–π stacking or a J-dimer via two

intermolecular hydrogen bond interactions between the nitro and amino functionalities (Figure S2, Supporting Information). Existing reports on the PNA dimeric structure have rather found their grounds on these two types of intermolecular interactions. In addition, a reported⁴⁸ single crystal structure indicated an oblique packing of the monomeric units in the unit cell (cf. Figure 2b) with both N–H–O and C–H–O intermolecular hydrogen bonds forcing the monomers to form a sheet parallel to the (101) plane, while individual sheets were interconnected via C–H–π interactions leading to a 3-dimensional network. However, to the best of our knowledge, no experimental validation to even the computationally predicted J-dimeric structure exists, leaving aside the O-dimer of PNA.

To obtain a deeper insight on the PNA dimeric structure, computations were performed at the DFT-M062X/6-31G+(d,p) level with IEFPCM in THF using single crystal coordinates.⁴⁸ The ground state optimized structure of the PNA dimer in Figure 2c shows its formation via a bifurcated H-bonding between the NH₂–NO₂ fragments. Many other members of the nitroaniline family, including 2-methyl-4-nitroaniline,⁴⁹ 2,4,6-trinitroaniline,⁵⁰ and 2,6-dichloro-4-nitroaniline,⁵¹ have shown similar bifurcated H-bond interaction in their single crystal structures. The computed dipole moments for the PNA monomer and dimer reflect the extent of charge transfer interaction in the ground state. A large increase in the dimeric dipole moment, slightly less than double that of the monomer (as in the case of a J-dimer), provides evidence for an oblique dimeric structure, while ruling out the earlier proposed centrosymmetric (cofacial-H) model of the PNA dimer with zero dipole moment.

Unlike the edge-to-face arrangement observed in smaller aromatics, this dimer conformation does not seem to have been facilitated through the quadrupolar electrostatic interaction between the hydrogen atoms and the aromatic benzene π-cloud. In the planar PNA dimer, to accommodate the maximum contact between the NH₂ and NO₂ groups, increased H–N–H and decreased O–N–O angles in reference to those of the monomer were observed (Table S1, Supporting Information). The planarity of the PNA O-dimer depicted in the XY-plane is evident from a very low N₁–N₂–N₃–N₄ dihedral angle ~90°. The relevant structural parameters for PNA monomer and dimer are provided in Table S1, Supporting Information. Thus, the ground state stabilization of the PNA O-dimer was attributed to three-centered/bifurcated intermolecular hydrogen bonding, while minimizing all other repulsive interactions. A detailed structure of the PNA O-dimer with respect to the slippage and polarization angles is discussed in the following section using the TDM of the monomeric electronic excitation.

To determine the energetics of dimer formation, the potential energy surface (PES) for the PNA dimer was

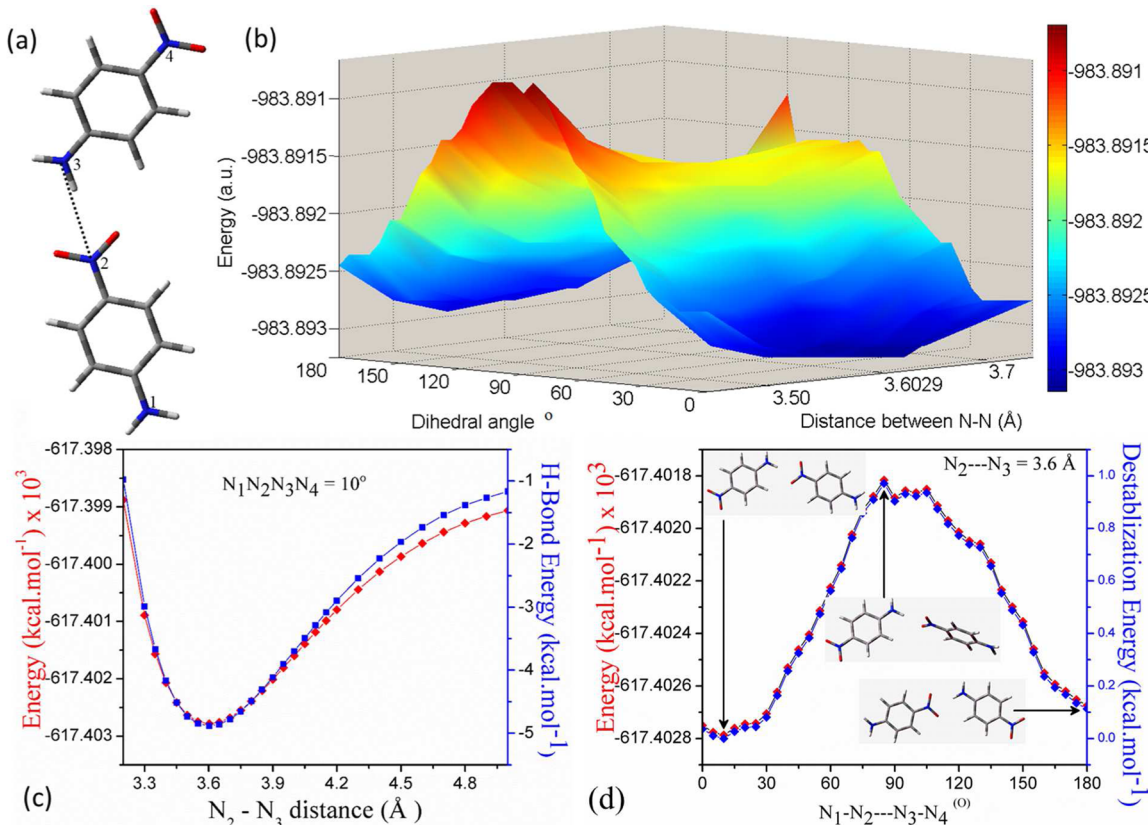


Figure 3. (a) DFT-M062X/6-31G+(d,p) with IEFPCM in THF optimized structure of the PNA dimer showing the $\text{N}_2\text{---N}_3$ distance along with the dihedral angle ($\text{N}_1\text{---N}_2\text{---N}_3\text{---N}_4$). (b) Computed potential energy surface of the PNA dimer as a function of the ($\text{N}_2\text{---N}_3$) distance and $\text{N}_1\text{---N}_2\text{---N}_3\text{---N}_4$ dihedral angle. (c) Computed potential energy curve (red trace) depicting stabilization energy of the dimer. The blue trace represents the intermolecular hydrogen bond energy estimated as [$E_{\text{dimer}} - (2E_{\text{monomer}})$]. Here, the contribution from $\pi\text{---}\pi$ stacking, though minor, cannot be ignored. (d) Variation of destabilization energy of the PNA O-dimer from its equilibrium structure with dihedral angle.

accurately computed as a function of distance between the donor amino and acceptor nitro nitrogens, and the dihedral angle ($\text{N}_1\text{---N}_2\text{---N}_3\text{---N}_4$) representing the angle between the PNA monomeric planes, Figure 3a. The conventionally used rigid scan method for the computation of monomeric PES requires molecular coordinates to be defined in a Z-matrix form whereas the relaxed scan method performs geometry optimization at each specified point. Because a Z-matrix cannot be defined for molecular dimers and the relaxed scan method is too expensive on the time scale for large molecular dimers, the PES for PNA dimer was obtained using single point energy calculations. Computations were performed at the DFT-M062X/6-31G+(d,p) level with IEFPCM in THF on the dimeric geometries obtained over 0–180° dihedral angles at intermolecular distances varying between 3.2 and 5.1 Å. The calculated energies for 259 nuclear configurations of the PNA O-dimer are tabulated in Table S2, Supporting Information. Consequently, the computed potential energy surface in Figure 3b depicts two minima, a global maximum, and a saddle point located on the scanned surface. The two minimum energy conformations were found to be almost isoenergetic, corresponding to planar dimeric structures with a $\text{N}_2\text{---N}_3$ distance at 3.60 Å for 10° and 180° $\text{N}_1\text{---N}_2\text{---N}_3\text{---N}_4$ dihedral angles. Of the two, the global minimum structure was assigned to the dimer geometry corresponding to a 10.0° dihedral angle. Subsequently, an out-of-plane dimeric conformation with a $\text{N}_2\text{---N}_3$ distance at 3.45 Å with an 85° $\text{N}_1\text{---N}_2\text{---N}_3\text{---N}_4$ dihedral angle represented a global energy maximum structure.

The potential energy curve for the PNA O-dimer as a function of $\text{N}_2\text{---N}_3$ distance was extracted from its ground state PES (Figure 3b) corresponding to a 10.0° dihedral angle. In Figure 3c, a 4.8 kcal mol⁻¹ dimer stabilization energy at an optimum $\text{N}_2\text{---N}_3$ distance of 3.60 Å was visualized. In contrast, whereas a much smaller stabilization energy of 3.0 kcal mol⁻¹ was reported for a centrosymmetrically packed PNA dimer/H-dimer,³⁷ for perfectly head-to-tail packed monomers/J-dimer,³⁶ a large dissociation energy of 5.0–11.4 kcal mol⁻¹ depending on the levels of calculation was observed. Though both results were obtained in a vacuum and at high levels of quantum mechanical calculations, the choice of initial models was rather based on assumptions than on an experimental evidence. As far as the $\text{N}_1\text{---N}_2\text{---N}_3\text{---N}_4$ dihedral angle is concerned, it is expected to affect the conformation of the PNA dimer, and therefore, an energy scan in Figure 3d depicts the destabilization energy of the dimer with rotation of a single PNA molecular fragment corresponding to the 0–180° range of dihedral angles. Surprisingly, the small drifts in the PNA dimeric nuclear geometries from its obliquely packed stable structure at 10° led to an increase in energy for all conformations shown. Nonetheless, the very small, but finite magnitude of increased energy with dihedral angle provides concrete evidence for a planar PNA dimer, supported by a three-centered intermolecular hydrogen bond. Along with this, the large distortion caused by a competition between the intermolecular hydrogen bonding and $\pi\text{---}\pi$ interaction ultimately results in an oblique structure of the PNA dimer.

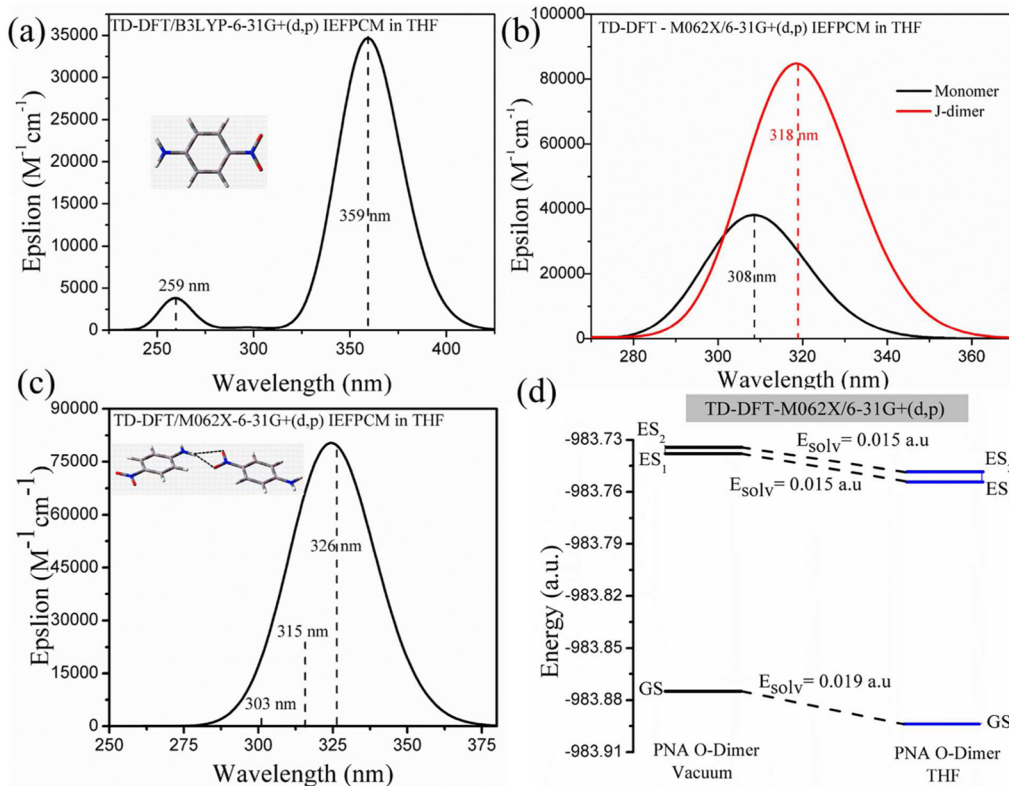


Figure 4. Computed UV–vis absorption spectrum of (a) PNA monomer and (b) PNA monomer and its J-dimer computed at TD-DFT-M062X/6-31G+(d,p)-IEFPCM in THF. (c) Computed UV–vis absorption spectrum of PNA O-dimer and (d) its energy level diagram in a vacuum and in THF solvent depicting a relatively better stabilization of the ground state (GS) than the excited states (ES).

Therefore, the energy minima on the PES can be safely assigned to PNA H- and J-dimeric structures, whereas the global minimum corresponds to the PNA O-dimer. Overall, the head-to-tail packed PNA O-dimer was thus visualized, showing major changes in the electronic structure accompanied by optical property changes, discussed in the subsequent sections.

Electron–Hole Density Distribution and Optical Absorption of the PNA O-Dimer in THF: Characteristics of the Photoexcited States. Single-electron excitation processes involve delocalization of an electron from A to B where A and B represent the real space functions. A commonly used model of an excited state corresponds to excitation of an electron from an occupied to a virtual MO (one electron model). However, excited states calculated herein demonstrate the electronic structure to be best described in terms of multiorbital electronic states with a linear combination of several occupied-to-virtual MO excitations. In view of the nonapplicability of a single orbital pair excitation model, the problem was circumvented by conceptualizing multimolecular orbital excitations in terms of electron and hole density distribution maps (EDD and HDD), providing very clear signatures for the monomeric and dimeric photoexcited states. Moreover, the generalized gradient approximation (GGA) based hybrid functional, B3LYP,⁴³ has been proven inaccurate toward accounting for the equilibrium dimeric structures, bonded via noncovalent interactions. Therefore, to correlate the PNA monomer properties with its dimer, computations on the PNA monomer were performed using the M062X functional.

Electronic structure calculation for the PNA monomer at TD-DFT-B3LYP/6-31G+(d,p) level with IEFPCM in THF predicted two major electronic transitions depicted in Figure

4a: the intense absorption band at $\lambda_m^1 = 359$ nm (3.45 eV) corresponding to $\pi-\pi^*$ ((HOMO \rightarrow LUMO), a single molecular orbital pair excitation) transition and the absorption at $\lambda_m^2 = 259$ nm involving a multimolecular orbital electronic excitation. This contradicts the much higher optical gap (4.05 eV) for PNA monomer computed at the MP2/6-31G+(d,p) level in a vacuum.³⁴ A computational analysis on the PNA J-dimer at the TD-DFT-M062X/6-31G+(d,p) level with IEFPCM in THF showed a single electronic transition at 318 nm, red-shifted relative to the 308 nm monomer excitation, Figure 4). In retrospect, the computed absorption spectrum of the PNA O-dimer at the same level of theory showed two major electronic transitions at 326 and 315 nm (cf. Figure 4c), validating the oblique dimeric structure, in line with the exciton model. Furthermore, the computed results in Figure 4d evidenced greater solvent stabilization of the dimeric ground state than of the excited states.

The computed 308 nm HOMO \rightarrow LUMO electronic transition for the PNA monomer at TD-DFT-M062X/6-31G+(d,p) level with IEFPCM in THF involved 97% weight (Figure 5a) for which the computed HDD map in Figure 5b shows a much denser isosurface localized on the amino group (compared to nitro), whereas the EDD map shows a denser isosurface on the nitro group. Therefore, the observed changes in the isosurface densities are attributed to electron density drift from an amino functionality toward the more polarizing nitro group. Further, the similarity of EDD and HDD maps with the ground state LUMO and HOMO isosurfaces of the PNA monomer can be attributed to a single MO pair excitation process. The computed configuration coefficients for allowed electronic excitations along with the centroid coordinates of

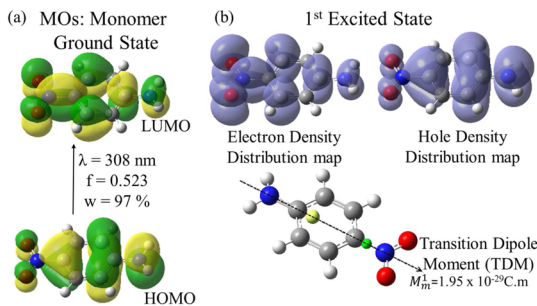


Figure 5. (a) Associated molecular orbitals, the oscillator strength and the weight of the 308 nm transition of the PNA monomer, computed via TD-DFT-M062X/6-31G+(d,p) level with IEFPCM in THF. (b) Electron (EDD) and hole (HDD) density distribution maps associated with the monomer excited state corresponding to 308 nm electronic transition. The direction of the monomeric transition dipole moment (M_m^1) with yellow and green spheres represents centroids of HDD and EDD maps.

EDD and HDD for PNA monomer are tabulated in Table 1, which were further used for computation of the TDM direction. Accordingly, the computed TDM direction is represented passing through the longer molecular axis of PNA monomer, pointing toward the nitro group. The calculated magnitude of TDM, $M_{308\text{nm}}^{\text{m(comp)}}$ amounted to $1.95 \times 10^{-29} \text{ C.m}$ using the relation⁵² $f = (8\pi^2 m_e v l M^2) / 3\hbar e^2$.

In Figure 6, electronic transitions for the PNA O-dimer at 326 and 315 nm corresponding to different configuration coefficients (Table S3, Supporting Information) show significant effect on their EDD and HDD maps. Similar electronic behavior has recently been cited for covalently bonded difluoroboraindacene (BODIPY) monomers in a BisBODIPY unit⁵³ with an energy difference of 0.47 eV between S_2 and S_3 states of BisBODIPY. A close examination of the frontier molecular orbitals involved in the electronic excitation of the ground state PNA O-dimer reveals that both LUMO and LUMO+1 possess much higher electron density localized on a single monomeric fragment. Nonetheless, it is worth noticing that the EDD maps for both the excited states resemble neither LUMO nor LUMO+1 of the ground state PNA dimer with EDD carrying almost equal electron density distribution on

both the monomeric units. Moreover, the EDD centroid for the 315 nm electronic excitation, being close to the central benzene ring of the hydrogen bond donor unit of PNA dimer, represents slightly more electron density drift, whereas that at 326 nm created significantly larger hole density localized on the acceptor unit. However, the 315 nm electron excitation resulted in homogeneous hole density distribution on both fragments, significantly affecting the direction of the associated transition dipole moments, as depicted in Figures 6a,b. The computed values of TDM, $M_{315\text{nm}}^{\text{d(comp)}}$ and $M_{326\text{nm}}^{\text{d(comp)}}$ amounted to 1.37×10^{-29} and $2.65 \times 10^{-29} \text{ C.m}$, respectively. These nonvanishing TDM magnitudes for both the electronic excitations support most promisingly the oblique geometry of the PNA O-dimer. Ideal cases of J-dimers in literature have been associated with almost double the value of monomeric TDM, whereas in the present investigation, the PNA O-dimeric structure is further justified with a TDM higher than the PNA monomer, but less than double its monomeric value (Table 1).

Aggregation of molecules in solution is most widely studied by optical spectroscopy. To investigate the possibility of dimerization/aggregation of PNA, we systematically studied the concentration dependent changes in the absorption spectra by concentrating the PNA solution in THF. The deconvoluted experimental UV-vis absorption spectrum of $1.7 \times 10^{-6} \text{ M}$ PNA in THF (cf. Figure 7a) shows major absorption bands centered at 235, 317, and 363 nm complying very well with the TD-DFT-B3LYP/6-31G+(d,p)-IEFPCM computed PNA monomer bands. However, increasing concentrations of PNA in THF facilitated intermolecular interaction/dimerization resulting in an asymmetrical band shape of the 363 nm absorption (Figure S5, Supporting Information), revealing the formation of PNA dimer in THF. The Beer–Lambert linearity was verified in the micromolar solutions of PNA in THF. Consequently, above a critical concentration of $0.19 \times 10^{-4} \text{ M}$, dimerization was enforced. Enhanced intermolecular hydrogen bonding in aprotic solvents⁵⁴ and the sparing solubility of PNA in THF⁵⁵ primarily stabilized the PNA dimer in THF.

The self-organized PNA monomers into dimeric aggregates in THF were characterized spectroscopically by a low intense $\lambda_d^1 = 377 \text{ nm}$ and a high intense $\lambda_d^2 = 355 \text{ nm}$ absorption band, visualized in the deconvoluted UV-vis absorption spectrum in

Table 1. Computed Centroid Coordinates and Distances between EDD and HDD Centroids for Allowed Excited State Transitions of PNA Monomer and the O-Dimer^a

	excited state	absorption wavelength (λ , nm), oscillator strength (f), transition dipole moment (M , C m)			centroid coordinates		
		λ	f	M	X (Å)	Y (Å)	Z (Å)
PNA monomer (m)	1	λ_m^1	308	EDD	1.269	0.000	0.004
		f	0.53	HDD	-1.346	0.000	-0.038
		M_m^1	1.95×10^{-29}	distance b/w centroids	2.615	0.000	0.034
	2	λ_m^2	229	EDD	0.433	0.000	0.005
PNA O-dimer (d)	1	f	0.1	HDD	-0.936	0.000	-0.017
		M_m^2	0.73×10^{-29}	distance b/w centroids	1.364	0.000	0.023
		λ_d^1	326	EDD	-0.131	0.054	0.007
	2	f	0.92	HDD	1.869	0.006	-0.011
		M_d^1	2.65×10^{-29}	distance b/w centroids	1.999	0.047	0.019
		λ_d^2	315	EDD	-1.582	-0.160	0.001
		f	0.25	HDD	0.373	0.253	0.007
		M_d^2	1.37×10^{-29}	distance b/w centroids	1.955	0.414	0.007

^aComputations were performed at M062X/6-31+G (d,p) with IEFPCM in THF using Multiwfn 3.44.

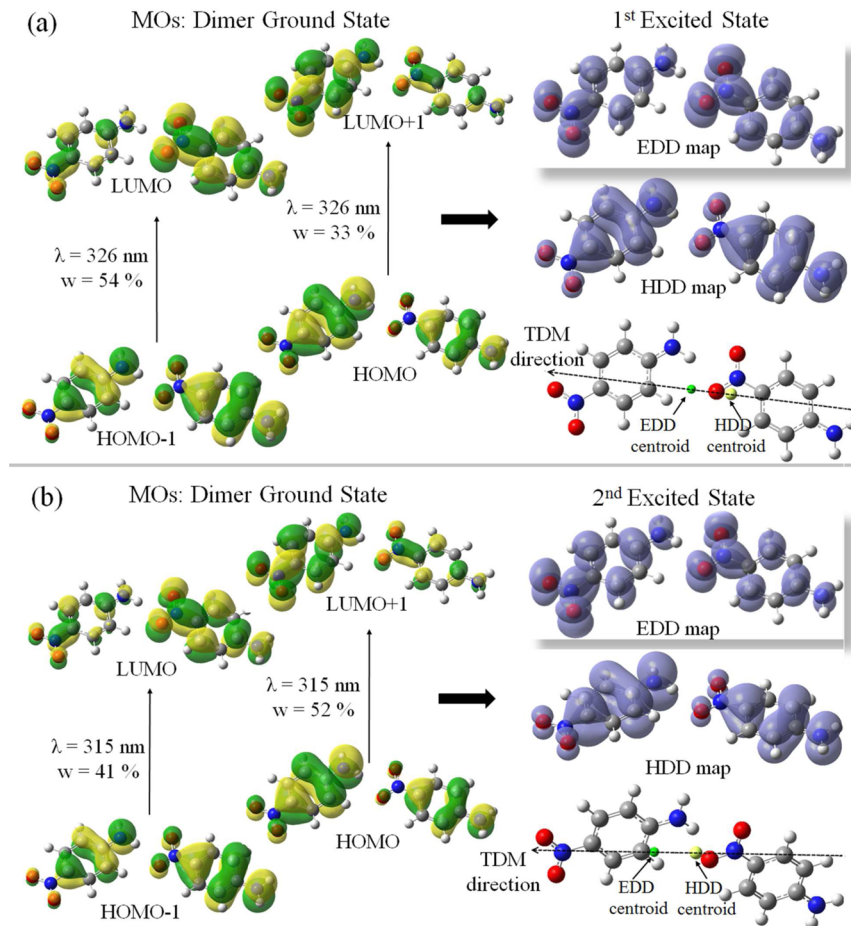


Figure 6. Electron (EDD) and hole (HDD) density distribution maps for electronic transitions in PNA O-dimer at (a) 326 nm and (b) 315 nm. Associated molecular orbitals and their corresponding weighing coefficients for both transitions are shown in left. Also shown are the transition dipole moment direction with yellow and green spheres representing HDD and EDD centroids.

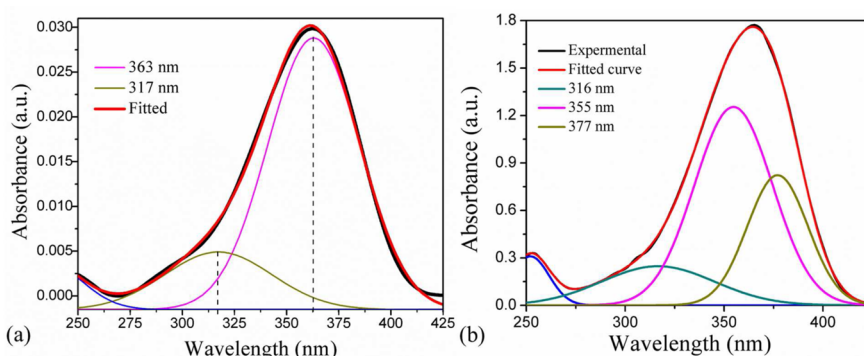


Figure 7. (a) Deconvoluted experimental UV-vis absorption spectrum of PNA monomer ($1.7 \times 10^{-6} \text{ M}$) in THF. (b) Deconvoluted experimental UV-vis absorption spectrum of PNA O-dimer in THF.

Figure 7b. The new bands are direct consequence of molecular aggregation and can be assigned to the dipole allowed electronic transitions to excitonic states of the dimer with the minor broad feature at 316 nm as a vibronic feature. Because these absorption bands are located symmetrically at both sides of the monomer absorption at 363 nm, excitonic coupling of two PNA monomers was instantaneously concluded to be the origin of O-dimer formation. It is noteworthy that irrespective of head-to-tail monomeric arrangement in the PNA dimer, the peculiarities in the dimeric structure make it have both blue- and red-shifted absorption bands validating the characteristic

O-dimer with net TDMs for both the electronic excitations carrying substantial weights. Recent years have also witnessed the discovery of similar spectral behavior attributed to the oblique stacking of monomers in the assemblies. The covalently bonded difluoroboraindacenones (BODIPY) monomers in a BisBODIPY unit⁵³ exhibited an absorption band dominated by two symmetrical bands centered around the monomeric BODIPY absorption. In the observed BisBODIPY conformation, the subunits were joined by a C–C bond with a 96.52° dihedral angle between the mean C_8BN_2 planes resulting in a noncancellation of transition dipole moment of the component

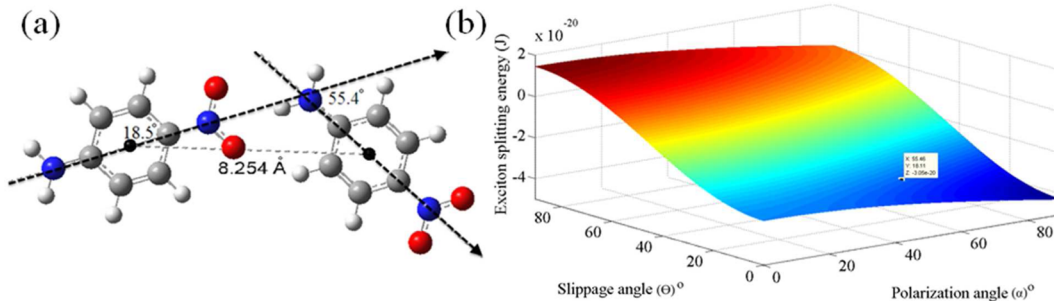


Figure 8. (a) Computed structure of PNA O-dimer at the DFT-M062X/6-31G+(d,p) level with IEFPCM in THF depicting the estimated slippage (18.5°) and polarization (55.4°) angles along with the internuclear distance (8.254 \AA). (b) Simulated exciton splitting energy surface for PNA O-dimeric aggregate ($n = 18$) as a function of slippage and polarization angles.

units (BODIPY). Similar spectral behavior was also observed for noncovalently bonded oligophenyleneethynylene (OPE)-BODIPY H-dimer in which the twisted dye conformation led to a 20° polarization angle.⁵⁶ Another example of O-dimer was reported as the fluorescent “H-type” dimer of merocyanine dyes.¹⁴ Despite being an H-dimer, the fluorescence behavior was attributed to a meager transition probability to the forbidden lower excited state caused by an extremely small rotational offset of 8° . To date, the oblique packing pattern of monomers in the dimers are interpreted in terms of rotational offset which is more precisely defined as a polarization angle in the exciton coupling model.

Exciton Splitting Energy of the PNA O-Dimer. The coupling of the transition dipole moments in the PNA O-dimer led to significant spectral signatures rationalized by exciton coupling theory. The molecular exciton coupling energy model is a state interaction theory where TDMs are considered as vectors and interaction between them is purely electrostatic.¹ Here, the excited state composite molecular energy levels that are nondegenerate in the individual molecule split, on the basis of the assumption that the direct overlap between the chromophoric molecular orbitals is negligible. Interaction between the excited states of the PNA monomer resulted in two distinct excited states for a dimer, separated by an energy gap defined as exciton splitting energy. In the PNA O-dimeric aggregate, the two allowed electronic transitions at 355 and 377 nm resulted in an exciton splitting energy of -1644 cm^{-1} . Similar exciton splitting energies have been reported in the literature for various conventional dye dimers.^{57–59}

An exact experimental match of exciton splitting energy with that from computation is difficult to establish. This is due to the deficiency in the exciton coupling model, based on the point-dipole approximation. Moreover, molecular level parameters i-e α , θ , N , and r cannot be accurately predicted using experimental methods. Consequently, the exciton splitting energy surface for the PNA O-dimer was traced using the computed structural parameters. Precise determination of intermolecular distance ($r = 8.254 \text{ \AA}$) along with slippage angle ($\theta = 18.5^\circ$) and polarization angle ($\alpha = 55.4^\circ$) were geometrically obtained from the ground state optimized PNA O-dimer structure in Figure 8a, substantiated with directions of monomeric TDMs from monomeric EDD and HDD maps, Figure 5b. The intermolecular distance r was accrued from two defined dummy positions placed on the monomeric TDM vectors, the angle between which defined the polarization angle $\alpha = 55.4^\circ$, as shown in Figure 8a. Although the head-to-tail arrangement of PNA monomers led to a slippage angle $\theta < 54.7^\circ$ in the O-dimer, a large distortion from a complete linear packing (as in J-

dimer) resulted in a large polarization angle. Kistler et al.⁶⁰ for a covalently bonded perylene diimide (PDI) dimeric complex have reported a large polarization angle of $\alpha = 86^\circ$ facilitated via through-space excitonic couplings. The computation thus signified the necessity of representing molecular electronic transitions in terms of EDD and HDD maps as they provided very accurate TDM directions for the computation of the above molecular parameters.

Bohn had reported⁶¹ a modified formalism to estimate the number of coherently coupled monomeric units N by correlating it with ΔE , the exciton splitting energy as

$$\Delta E = \frac{2 |M|^2 (\cos \alpha - 3 \cos^2 \theta) \left(1 - \frac{1}{N}\right)}{4\pi\epsilon r^3} \quad (3)$$

or

$$\Delta E = \frac{2}{4\pi\epsilon} \frac{3he^2f\lambda}{8\pi^2 m_e c} \frac{(\cos \alpha - 3 \cos^2 \theta)}{r^3} \frac{(N-1)}{N} \quad (4)$$

where M , f , and λ are the TDM, oscillator strength, and absorption wavelength for the monomeric electronic excitation and r , θ , and α carry the usual meaning. Consequently, N for the PNA O-dimeric aggregate was estimated to be 18 upon compliance of the computed ΔE (eq 4) with the experimental $\Delta E \sim 1644 \text{ cm}^{-1}$. Accordingly, the exciton splitting energy surface for the PNA O-dimer was traced as a function of r , θ , and α in Figure 8b. However, this aggregation number does not relate to the physical size, but to the number of molecules in the aggregate that underwent mutual spectral perturbation. Exciton delocalization in a coherent domain of ~ 70 molecules was observed for pseudoisocyanine aggregates using pump-probe spectroscopy experiments at 1.7 K .⁶² In the case of 5,5',6,6'-tetrachloro-1,1'-diethyl-3, 3'-di(4-sulfonylbutyl)-benzimidazolocarbocyanine J-aggregates, an exciton delocalization length over ~ 16 molecules at room temperature was determined by femtosecond nonlinear optical experiments.⁶³ In the present investigation, 18 PNA monomeric units/9 PNA O-dimers were thus established to constitute the repeating spectroscopic unit cell of the PNA O-dimeric aggregate, corroborating both experimental and computational data.

Excited State Equilibrium Structures of the PNA O-Dimer: Emission Characteristics. The nitro ($-\text{NO}_2$) group is well-known for reducing fluorescence in the majority of aromatic compounds via nonradiative processes and the behavior was witnessed for PNA monomer in THF. Much to our surprise, the dimeric form in THF solution was observed to be slightly emissive in the visible region. The PNA O-dimer differs from both the H- and J-dimer in terms of its

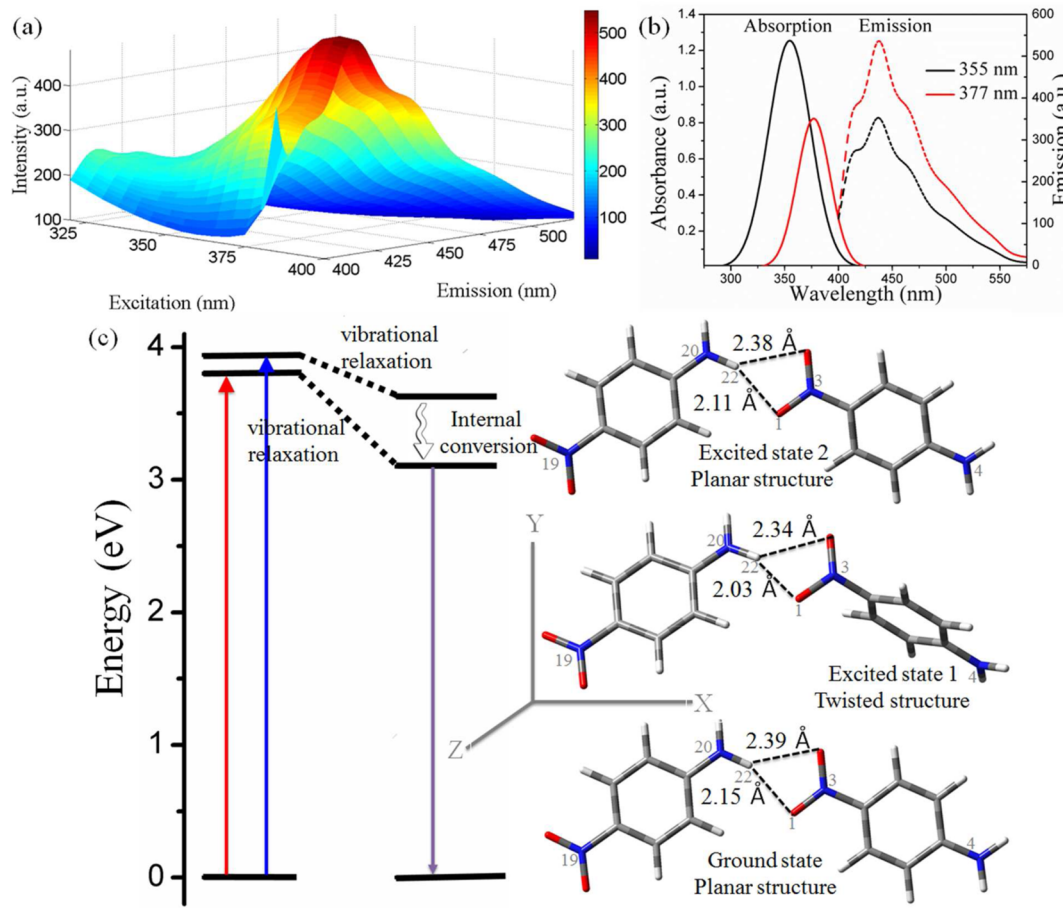


Figure 9. (a) Emission spectra of PNA dimer in THF obtained in matrix scan emission experiment. (b) Absorption characteristics (solid red and black) of PNA O-dimer in THF and corresponding emission spectra (dotted red and black) of PNA O-dimer. (c) Probable de-excitation/geometry relaxation modes of the excited dimer from its computed equilibrium structure of ground and excited states. Shown in figure are the 326 and 315 nm excitations, emitting exclusively at 400 nm.

nonvanishing TDMs for both the electronic excitations, evident in the experimentally obtained steady state matrix scan emission spectra in Figure 9a. The very broad and structureless emission spectra depicted continuous emission intensity increase at 435 nm with increasing excitation wavelength, with a finite contribution from the solvent dependent vibronic progression.

The contour map of the recorded emission intensities depicted in Figure S6 (Supporting Information) further supports the above observation. Moreover, from Figure 9b it can be interpreted, with reference to a much larger excited state population, the emission being low, as evidence for a nonradiative decay of the PNA O-dimer to a lower lying excited state followed by a subsequent radiative decay. Furthermore, a pronounced experimental Stoke's shift of 58 nm from 377 nm absorption to 435 nm emission wavelength hints toward a definite geometry relaxation of the PNA O-dimeric excited structure. It was therefore necessary to carry out excited state computations of the PNA O-dimer to arrive at equilibrium structures in this regard.

The excited state equilibrium structures and emission maxima of PNA O-dimer have been computed at TD-DFT-M062X/6-31G+(d,p) level with IEFPCM in THF, complying with the experimental observation in Figure 9b. For the excited state structure computation in solution, a clear distinction exists between equilibrium and nonequilibrium methods where the

solvent responds in two different ways to the changes in the solute state: (i) it polarizes its electron distribution via a very rapid process and (ii) the solvent molecules reorient themselves via rotation, a much slower process. An equilibrium calculation therefore describes a situation where the solvent has time to fully respond to the solute in both ways, e.g., a geometry optimization, a process that takes place on the same time scale as molecular motion in the solvent. A nonequilibrium calculation is appropriate for processes that are too rapid for the solvent to have time to fully respond, e.g., a vertical electronic excitation. Equilibrium solvation is the generally adopted solvation method for TD-DFT excited state geometry optimizations, whereas TD-DFT energy computation involves the nonequilibrium solvation model.

Due to the large size of PNA dimer, the widespread use of more conventional excited state methods, such as MR-CI and CASPT2 approaches were not feasible because of their unfavorable scaling with molecular size. Furche and Ahlrichs found TD-DFT to be more accurate for the low-lying excited state geometries of typical molecules than CIS or TD-HF.⁶⁴ Furthermore, the photostability of D-π-A sensitizers, the excited state geometries and emission maxima of 11 organic dyes have also been explored at TD-DFT level using M062X-linear response-IEFPCM.⁶⁵ More recently, emission peak wavelength, spectral line shape, and the Stokes's shift of an organic chromophore 4-naphthoyloxy-1-methoxy-2,6,6-tetra-

methylpiperidine (*N*fo-TEMPO-Me) in toluene solution was explored through an integrated computational strategy combining a classical dynamic sampling with a quantum mechanical description at TD-DFT level.⁶⁶ Therefore, excited state structures of PNA O-dimer for 326 and 315 nm electronic excitations were first computed at the TD-DFT/M062X/6-31G+(d,p) level with IEFPCM in THF, which defaults to nonequilibrium solvation. Here, the stability of molecular excited states permits an emission of the molecule to occur from a vibrationally relaxed excited state in an equilibrium solvent reaction field. Therefore, to find the minimum energy point on the excited state potential energy surface, TD-DFT geometry optimizations were performed on the obtained excited state structures with equilibrium and linear response solvation. Finally, in this framework, the emission maximum was evaluated as a difference between the energies of the optimized ground state structure and the equilibrium excited state of the PNA O-dimer.

The computed conformational behavior of PNA O-dimeric excited state equilibrium structures on 326 and 315 electronic excitations is depicted in Figure 9c. To our knowledge, no experimental and computed excited state structures were so far reported for these dimers. The most relevant changes in structural parameters for the computed PNA dimeric excited states were related to bond lengths and bond angles with their variations summarized in Table S4 (Supporting Information). Quantification of the vibrationally relaxed excited states followed by equilibrium solvation could be clearly visualized in terms of their relative energies with respect to the ground state dimeric structure. Moreover, vibrational relaxation led to large changes in hydrogen bond lengths for the PNA dimeric excited states; changes as large as 0.12 and 0.04 Å were found in O₁—H₂₂ length for first and second dimeric excited states, respectively. Instead, negligible modifications were found for O₂—H₂₂ intermolecular hydrogen bond lengths. A substantial deviation from the coplanarity of the PNA dimeric excited states was evident from the twisting of N₁₉—N₂₀—N₃—N₄ dihedral angle, characterizing the relative orientation of the two PNA fragments in the dimer. Moreover, the observed molecular rigidity of the benzene structure blocked the competing radiationless deactivation channels. A computed Stoke's shift of 74 nm (~0.7 eV) resulted from the pronounced vibrational relaxation of the lower lying dimeric excited state in the vicinity of the twisted equilibrium structure of the excited state, visualized in Figure 9c.

Most remarkably, the 435 nm emission band with much larger emission intensity upon 377 nm excitation in comparison with 355 nm excitation provides unequivocal evidence that the PNA dimer emission originates from the lower exciton state. When the energy gap between the shorter and longer wavelength bands becomes larger, a slower internal conversion between the second and first excited states is expected.⁶⁷ An energy separation of 0.52 eV between the PNA dimeric excited states being small, radiationless decay from the higher excited state is expected to be fast. An anomalous S₂ emission for BODIPY derivatives was recently attributed to a large energy gap of 1.3 eV between the S₁ and S₂ states.⁶⁸ However, in contravention of Kasha's rule,⁶⁹ few reports related to S₂-exciton dynamics of porphyrin J-aggregates⁷⁰ showed the S₂ fluorescence to be almost quenched although the energy separation between S₁ and S₂ states was still appreciable (0.78 eV). This was explained mainly by the N—H stretching vibration, which acted as an accepting mode of the electronic

excitation energy. Overall, the radiative decay of PNA O-dimer from the corresponding electronically excited states precedes the nonradiative decay of the higher energy excited state via internal conversion, as shown in Figure 9c. The results implied that the use of the TD-DFT/PCM method in computing the low-lying excited states of the PNA O-dimer allowed obtaining emission data comparing well with the experimental values. The possibility to use TD-DFT in obtaining equilibrium excited state geometries and reproducing the emission maxima opens the way to the study of the excited state potential energy surfaces of various nitroaniline dyes and evaluation of their photostability. This in turn may open up the possibility to design improved compounds in terms of excited state stability through substitutions and/or insertion of different molecular units.

CONCLUSIONS

Given the planar structure of PNA, it was not initially anticipated that oblique aggregates of the PNA molecule could be formed. Our present investigation contradicts the common perception and finding that PNA forms an H- or J-dimer. The PNA O-dimer geometry optimized via the DFT-M062X/6-31G+(d,p)-IEFPCM calculation, the spectroscopic studies, and the X-ray crystallographic data showed a perfect O-dimer unit as the energetically preferred geometry. *p*-Nitroaniline formed O-dimer in the aprotic solvent THF with slippage and polarization angles of 18.5° and 55.4°, respectively. The oblique packing was supported from the bifurcated hydrogen bonding with a stabilization energy of 4.8 kcal mol⁻¹ at room temperature with significant contribution from the π–π interaction. The arrangement of *p*-nitroaniline monomers into an O-dimer led to exchange of excitation energy between the two monomeric units with a splitting of the energy level separated by an interaction energy of -1644 cm⁻¹. UV-vis absorption and electronic structure calculation of the PNA dimer showed two intense absorption bands at 355 and 377 nm, characteristic of the oblique-type geometry. The non-vanishing transition dipole moments for both electronic transitions in the dimer, computed using electron–hole pair density distribution maps, showed significant changes in their direction and magnitude as well. The pronounced vibrational relaxation of the lower excited state in conjunction with internal conversion of the vibrationally relaxed higher energy excited state explained the single emission wavelength for the PNA O-dimeric aggregate. The exciton coupling energy between the 18 close-packed neighboring PNA monomers and the structural parameters of the O-dimeric aggregate, computed using Kasha's exciton model, complied with the observed spectral shifts in the absorption spectra. In conclusion, using computational strategies for the investigation of molecular dimers, we can devise futuristic molecular aggregates with tailored properties.

ASSOCIATED CONTENT

S Supporting Information

Energy level diagram, optimized structures, UV-vis absorption spectra of PNA in THF with varying concentrations, and contour map of PNA dimer obtained in matrix scan emission spectra are provided. Tables summarizing monomer and dimeric ground state structural parameters, single point energies computed for 259 nuclear geometries of PNA dimer, TD-DFT-M062X/6-31G+(d,p)-IEFPCM in THF computed electronic transitions for PNA O-dimer, and structural parameters for PNA dimeric excited states are provided. The

Supporting Information is available free of charge on the ACS Publications website at DOI: 10.1021/acs.jpca.5b03645.

AUTHOR INFORMATION

Corresponding Author

*A. Patnaik. Fax: (+91) 2257 4202. E-mail: archita59@yahoo.com.

Notes

The authors declare no competing financial interest.

ACKNOWLEDGMENTS

N.A. thanks CSIR, New Delhi, for providing a Research Fellowship. P. G. Senapathy center for computing resources, IIT-Madras, is gratefully acknowledged for providing excellent computing facility.

REFERENCES

- (1) Kasha, M.; Rawls, H. R.; El-Bayoumi, A. The Exciton Model in Molecular Spectroscopy. *Pure Appl. Chem.* **1965**, *11*, 371–392.
- (2) Place, I.; Perlstein, J.; Penner, T. L.; Whitten, D. G. Stabilization of the Aggregation of Cyanine Dyes at the Molecular and Nanoscopic Level†. *Langmuir* **2000**, *16*, 9042–9048.
- (3) Valleau, S.; Saikin, S. K.; Yung, M.-H.; Guzik, A. A. Exciton Transport in Thin-Film Cyanine Dye J-Aggregates. *J. Chem. Phys.* **2012**, *137*, 034109.
- (4) Marciniak, H.; Li, X.-Q.; Würthner, F.; Lochbrunner, S. One-Dimensional Exciton Diffusion in Perylene Bisimide Aggregates. *J. Phys. Chem. A* **2011**, *115*, 648–654.
- (5) Son, M.; Park, K. H.; Shao, C.; Würthner, F.; Kim, D. Spectroscopic Demonstration of Exciton Dynamics and Excimer Formation in a Sterically Controlled Perylene Bisimide Dimer Aggregate. *J. Phys. Chem. Lett.* **2014**, *5*, 3601–3607.
- (6) Nüesch, F.; Moser, J. E.; Shklover, V.; Grätzel, M. Merocyanine Aggregation in Mesoporous Networks. *J. Am. Chem. Soc.* **1996**, *118*, 5420–5431.
- (7) Shankar, B. V.; Patnaik, A. J-Aggregates in Matrix Stabilized Two-Dimensional Azobenzene Derivatives. *J. Colloid Interface Sci.* **2006**, *302*, 259–266.
- (8) Shankar, B. V.; Patnaik, A. Surface Pressure Driven Supramolecular Architectures from Mixed H-Aggregates of Dye-Capped Azobenzene Derivative. *Langmuir* **2006**, *22*, 4758–4765.
- (9) Kumar, K. S.; Patnaik, A. Solvent-Polarity-Tunable Dimeric Association of a Fullerene (C₆₀)–N,N-Dimethylaminoazobenzene Dyad: Modulated Electronic Coupling of the Azo Chromophore with a Substituted 3d Fullerene. *Chem. - Eur. J.* **2011**, *17*, 5327–5343.
- (10) Möbius, D. Scheibe Aggregates. *Adv. Mater.* **1995**, *7*, 437–444.
- (11) del Valle, J. C.; Catalán, J.; Amat-Guerri, F. Comparative Photophysical Study of Rose Bengal, Eosin Y and Their Monomethyl and Dimethyl Derivatives. *J. Photochem. Photobiol., A* **1993**, *72*, 49–53.
- (12) Rabinowitch, E.; Epstein, L. F. Polymerization of Dyestuffs in Solution. Thionine and Methylene Blue I. *J. Am. Chem. Soc.* **1941**, *63*, 69–78.
- (13) West, W.; Pearce, S. The Dimeric State of Cyanine Dyes. *J. Phys. Chem.* **1965**, *69*, 1894–1903.
- (14) Rösch, U.; Yao, S.; Wortmann, R.; Würthner, F. Fluorescent H-Aggregates of Merocyanine Dyes. *Angew. Chem., Int. Ed.* **2006**, *45*, 7026–7030.
- (15) Gierschner, J.; Lüer, L.; Milián-Medina, B.; Oelkrug, D.; Egelhaaf, H.-J. Highly Emissive H-Aggregates or Aggregation-Induced Emission Quenching? The Photophysics of All-Trans Para-Distyrylbenzene. *J. Phys. Chem. Lett.* **2013**, *4*, 2686–2697.
- (16) Varghese, S.; Park, S. K.; Casado, S.; Fischer, R. C.; Resel, R.; Milián-Medina, B.; Wannemacher, R.; Park, S. Y.; Gierschner, J. Stimulated Emission Properties of Sterically Modified Distyrylbenzene-Based H-Aggregate Single Crystals. *J. Phys. Chem. Lett.* **2013**, *4*, 1597–1602.
- (17) Czikkely, V.; Forsterling, H. D.; Kuhn, H. Extended Dipole Model for Aggregates of Dye Molecules. *Chem. Phys. Lett.* **1970**, *6*, 207–210.
- (18) Bureš, F.; Schweizer, W. B.; May, J. C.; Boudon, C.; Gisselbrecht, J.-P.; Gross, M.; Biaggio, I.; Diederich, F. Property Tuning in Charge-Transfer Chromophores by Systematic Modulation of the Spacer between Donor and Acceptor. *Chem. - Eur. J.* **2007**, *13*, 5378–5387.
- (19) Bureš, F.; Pytela, O.; Kivala, M.; Diederich, F. Solvatochromism as an Efficient Tool to Study N,N-Dimethylamino- and Cyano-Substituted II-Conjugated Molecules with an Intramolecular Charge-Transfer Absorption. *J. Phys. Org. Chem.* **2011**, *24*, 274–281.
- (20) Kyaw, A. K. K.; Wang, D. H.; Wynands, D.; Zhang, J.; Nguyen, T.-Q.; Bazan, G. C.; Heeger, A. J. Improved Light Harvesting and Improved Efficiency by Insertion of an Optical Spacer (ZnO) in Solution-Processed Small-Molecule Solar Cells. *Nano Lett.* **2013**, *13*, 3796–3801.
- (21) Green, M. A.; Emery, K.; Hishikawa, Y.; Warta, W.; Dunlop, E. D. Solar Cell Efficiency Tables (Version 40). *Prog. Photovoltaics* **2012**, *20*, 606–614.
- (22) Kan, Bin; Liu, Feng; Long, Guankui; Wan, Xiangjian; Chen, Xiaojing; Zuo, Yi; Ni, Wang; Zhang, Huijing; Li, Miaomiao; Zhang, Q.; et al. Small-Molecule Solar Cells with Efficiency over 9%. *Nat. Photonics* **2015**, *9*, 35–41.
- (23) Fang, Y.; Pandey, A. K.; Nardes, A. M.; Kopidakis, N.; Burn, P. L.; Meredith, P. A Narrow Optical Gap Small Molecule Acceptor for Organic Solar Cells. *Adv. Energy Mater.* **2013**, *3*, 54–59.
- (24) An, B.-K.; Gierschner, J.; Park, S. Y. II-Conjugated Cyanostilbene Derivatives: A Unique Self-Assembly Motif for Molecular Nanostructures with Enhanced Emission and Transport. *Acc. Chem. Res.* **2012**, *45*, 544–554.
- (25) Varghese, S.; Das, S. Role of Molecular Packing in Determining Solid-State Optical Properties of II-Conjugated Materials. *J. Phys. Chem. Lett.* **2011**, *2*, 863–873.
- (26) Kanoun, M. B.; Champagne, B. Calculating the Second-Order Nonlinear Optical Susceptibilities of 3-Methyl-4-Nitropyridine N-Oxide, 2-Carboxylic Acid-4-Nitropyridine-1-Oxide, 2-Methyl-4-Nitroaniline, and M-Nitroaniline Crystals. *Int. J. Quantum Chem.* **2011**, *111*, 880–890.
- (27) Williams, D. J. Organic Polymeric and Non-Polymeric Materials with Large Optical Nonlinearities. *Angew. Chem., Int. Ed. Engl.* **1984**, *23*, 690–703.
- (28) Sureshkumar, M. S.; Goyal, R. K.; Negi, Y. S.; Pratheepkumar, A.; Reddy, K. R.; Singh, R. P.; Dodge, J. W.; Aiyer, R. C. Studies on the Feasibility of Recycled Polystyrene Doped with Nlo Active Meta-Nitroaniline for Optoelectronics Applications. *Polym. Adv. Technol.* **2011**, *22*, 1865–1871.
- (29) Oudar, J. L.; Zyss, J. Structural Dependence of Nonlinear-Optical Properties of Methyl-(2,4-Dinitrophenyl)-Aminopropanoate Crystals. *Phys. Rev. A: At., Mol., Opt. Phys.* **1982**, *26*, 2016–2027.
- (30) Zyss, J.; Nicoud, J. F.; Coquillay, M. Chirality and Hydrogen Bonding in Molecular Crystals for Phase-Matched Second-Harmonic Generation: N-(4-Nitrophenyl)-(L)-Prolinol (Npp). *J. Chem. Phys.* **1984**, *81*, 4160–4167.
- (31) Etter, M. C.; Reutzel, S. M. Hydrogen Bond Directed Cocrystallization and Molecular Recognition Properties of Acyclic Imides. *J. Am. Chem. Soc.* **1991**, *113*, 2586–2598.
- (32) Etter, M. C.; Urbanczyk-Lipkowska, Z.; Zia-Ebrahimi, M.; Panunto, T. W. Hydrogen Bond-Directed Cocrystallization and Molecular Recognition Properties of Diarylureas. *J. Am. Chem. Soc.* **1990**, *112*, 8415–8426.
- (33) Yuan-Hong, S.; Jing, L.; Ke, Z.; Chuan-Kui, W. The Aggregation Effects on the Two-Photon Absorption Properties of Para-Nitroaniline Polymers by Hydrogen-Bond Interactions. *Chin. Phys. B* **2010**, *19*, 044207.
- (34) Datta, A.; Pati, S. K. Dipolar Interactions and Hydrogen Bonding in Supramolecular Aggregates: Understanding Cooperative Phenomena for 1st Hyperpolarizability. *Chem. Soc. Rev.* **2006**, *35*, 1305–1323.

- (35) Panunto, T. W.; Urbanczyk-Lipkowska, Z.; Johnson, R.; Etter, M. C. Hydrogen-Bond Formation in Nitroanilines: The First Step in Designing Acentric Materials. *J. Am. Chem. Soc.* **1987**, *109*, 7786–7797.
- (36) Moliner, V.; Escribano, P.; Peris, E. Intermolecular Hydrogen Bonding in Nlo. Theoretical Analysis of the Nitroaniline and Hf Cases. *New J. Chem.* **1998**, *22*, 387–392.
- (37) Di Bella, S.; Lanza, G.; Fragalà, I.; Yitzchaik, S.; Ratner, M. A.; Marks, T. J. Charge Distribution and Second-Order Nonlinear Optical Response of Charged Centrosymmetric Chromophore Aggregates. An Ab Initio Electronic Structure Study of P-Nitroaniline Dimers. *J. Am. Chem. Soc.* **1997**, *119*, 3003–3006.
- (38) Helttunen, K.; Lehtovaara, L.; Häkkinen, H.; Nissinen, M. Crystal Structures and Density Functional Theory Calculations of O- and P-Nitroaniline Derivatives: Combined Effect of Hydrogen Bonding and Aromatic Interactions on Dimerization Energy. *Cryst. Growth Des.* **2013**, *13*, 3603–3612.
- (39) Nakatsuji, H.; Caricato, M.; Li, Xiaosong; Hratchian, H. P.; Izmaylov, Artur, F.; Bloino, Julien; Zheng, G.; Sonnenberg, J. L.; Hada, M.; Frisch, M. J.; et al. Gaussian 09; Gaussian, Inc.: Wallingford, CT, USA, 2009.
- (40) Charaf-Eddin, A.; Planchat, A.; Mennucci, B.; Adamo, C.; Jacquemin, D. Choosing a Functional for Computing Absorption and Fluorescence Band Shapes with Td-Dft. *J. Chem. Theory Comput.* **2013**, *9*, 2749–2760.
- (41) Leang, S. S.; Zahariev, F.; Gordon, M. S. Benchmarking the Performance of Time-Dependent Density Functional Methods. *J. Chem. Phys.* **2012**, *136*, 104101.
- (42) Isegawa, M.; Peverati, R.; Truhlar, D. G. Performance of Recent and High-Performance Approximate Density Functionals for Time-Dependent Density Functional Theory Calculations of Valence and Rydberg Electronic Transition Energies. *J. Chem. Phys.* **2012**, *137*, 244104.
- (43) Zhao, Y.; Truhlar, D. The M06 Suite of Density Functionals for Main Group Thermochemistry, Thermochemical Kinetics, Non-covalent Interactions, Excited States, and Transition Elements: Two New Functionals and Systematic Testing of Four M06-Class Functionals and 12 Other Functionals. *Theor. Chem. Acc.* **2008**, *120*, 215–241.
- (44) Ray, P. C.; Leszczynski, J. Nonlinear Optical Properties of Highly Conjugated Push–Pull Porphyrin Aggregates: Role of Intermolecular Interaction. *Chem. Phys. Lett.* **2006**, *419*, 578–583.
- (45) Cheng, W. D.; Wu, D. S.; Zhang, H.; Li, X. D.; Chen, D. G.; Lang, Y. Z.; Zhang, Y. C.; Gong, Y. J. First Principle Treatments on Site- and Size-Dependent Supramolecular Interactions and Nonlinear Optical Properties of Polymer of 2-Methyl-4-Nitroaniline. *J. Phys. Chem. B* **2004**, *108*, 12658–12664.
- (46) Lu, T.; Chen, F. Multiwfns: A Multifunctional Wavefunction Analyzer. *J. Comput. Chem.* **2012**, *33*, 580–592.
- (47) Lu, T. C.; Chen, F.-W. Calculation of Molecular Orbital Composition. *Acta Chim. Sinica* **2011**, *69*, 2393–2406.
- (48) Qian, H.-Y.; Yin, Z.-G.; Jia, J.; Zhou, N.; Feng, L.-Q. 4-Nitroaniline: A Redetermination. *Acta Crystallogr., Sect. E: Struct. Rep. Online* **2006**, *62*, o5048–o5049.
- (49) Lipscomb, G. F.; Garito, A. F.; Narang, R. S. An Exceptionally Large Linear Electro-Optic Effect in the Organic Solid Mn. *J. Chem. Phys.* **1981**, *75*, 1509–1516.
- (50) Holden, J. R.; Dickinson, C.; Bock, C. M. Crystal Structure of 2,4,6-Trinitroaniline. *J. Phys. Chem.* **1972**, *76*, 3597–3602.
- (51) Hughes, D. L.; Trotter, J. Crystal Structure of 2,6-Dichloro-4-Nitroaniline. *J. Chem. Soc. A* **1971**, 2181–2184.
- (52) Hilborn, R. C. Einstein Coefficients, Cross Sections, F Values, Dipole Moments, and All That. *Am. J. Phys.* **1982**, *50*, 982–986.
- (53) Bröring, M.; Krüger, R.; Link, S.; Kleeburg, C.; Köhler, S.; Xie, X.; Ventura, B.; Flamigni, L. Bis(Bf₂)-2,2'-Bidipyrins (Bisbodipys): Highly Fluorescent Bodipy Dimers with Large Stokes Shifts. *Chem. - Eur. J.* **2008**, *14*, 2976–2983.
- (54) Würthner, F.; Thalacker, C.; Sautter, A.; Schärtl, W.; Ibach, W.; Hollricher, O. Hierarchical Self-Organization of Perylene Bisimide—Melamine Assemblies to Fluorescent Mesoscopic Superstructures. *Chem. - Eur. J.* **2000**, *6*, 3871–3886.
- (55) François Huyskens, H. M.; Huyskens, P. Solubilities of P-Nitroanilines in Various Classes of Solvents. Specific Solute-Solvent Interactions. *J. Mol. Struct.* **1998**, *441*, 17–25.
- (56) Allampally, N. K.; Florian, A.; Mayoral, M. J.; Rest, C.; Stepanenko, V.; Fernández, G. H-Aggregates of Oligophenylenethiophylene (Ope)-Bodipy Systems in Water: Guest Size-Dependent Encapsulation Mechanism and Co-Aggregate Morphology. *Chem. - Eur. J.* **2014**, *20*, 10669–10678.
- (57) Würthner, F.; Yao, S.; Debaerdemaeker, T.; Wortmann, R. Dimerization of Merocyanine Dyes. Structural and Energetic Characterization of Dipolar Dye Aggregates and Implications for Nonlinear Optical Materials. *J. Am. Chem. Soc.* **2002**, *124*, 9431–9447.
- (58) Osuka, A.; Maruyama, K. Synthesis of Naphthalene-Bridged Porphyrin Dimers and Their Orientation-Dependent Exciton Coupling. *J. Am. Chem. Soc.* **1988**, *110*, 4454–4456.
- (59) Kistler, K. A.; Pochas, C. M.; Yamagata, H.; Matsika, S.; Spano, F. C. Absorption, Circular Dichroism, and Photoluminescence in Perylene Diimide Bichromophores: Polarization-Dependent H- and J-Aggregate Behavior. *J. Phys. Chem. B* **2012**, *116*, 77–86.
- (60) Thompson, M. A.; Zerner, M. C.; Fajer, J. A. Theoretical Examination of the Electronic Structure and Excited States of the Bacteriochlorophyll B Dimer from Rhodopseudomonas Viridis. *J. Phys. Chem.* **1991**, *95*, 5693–5700.
- (61) Bohn, P. W. Aspects of Structure and Energy Transport in Artificial Molecular Assemblies. *Annu. Rev. Phys. Chem.* **1993**, *44*, 37–60.
- (62) Knoester, J. Nonlinear Optical Line Shapes of Disordered Molecular Aggregates: Motional Narrowing and the Effect of Intersite Correlations. *J. Chem. Phys.* **1993**, *99*, 8466–8479.
- (63) Moll, J.; Daehne, S.; Durrant, J. R.; Wiersma, D. A. Optical Dynamics of Excitons in J Aggregates of a Carbocyanine Dye. *J. Chem. Phys.* **1995**, *102*, 6362–6370.
- (64) Furche, F.; Ahlrichs, R. Adiabatic Time-Dependent Density Functional Methods for Excited State Properties. *J. Chem. Phys.* **2002**, *117*, 7433–7447.
- (65) Bernini, C.; Zani, L.; Calamante, M.; Reginato, G.; Mordini, A.; Taddei, M.; Basosi, R.; Sinicropi, A. Excited State Geometries and Vertical Emission Energies of Solvated Dyes for Dssc: A Pcm/Td-Dft Benchmark Study. *J. Chem. Theory Comput.* **2014**, *10*, 3925–3933.
- (66) De Mitri, N.; Monti, S.; Prampolini, G.; Barone, V. Absorption and Emission Spectra of a Flexible Dye in Solution: A Computational Time-Dependent Approach. *J. Chem. Theory Comput.* **2013**, *9*, 4507–4516.
- (67) Steer, R. P.; Ramamurthy, V. Photophysics and Intramolecular Photochemistry of Thiones in Solution. *Acc. Chem. Res.* **1988**, *21*, 380–386.
- (68) Cho, D. W.; Fujitsuka, M.; Ryu, J. H.; Lee, M. H.; Kim, H. K.; Majima, T.; Im, C. S2 Emission from Chemically Modified Bodipys. *Chem. Commun.* **2012**, *48*, 3424–3426.
- (69) Kasha, M. Characterization of Electronic Transitions in Complex Molecules. *Discuss. Faraday Soc.* **1950**, *9*, 14–19.
- (70) Misawa, K.; Kobayashi, T. Ultrafast Exciton and Excited-Exciton Dynamics in J-Aggregates of Three-Level Porphyrin Molecules. *J. Chem. Phys.* **1999**, *110*, 5844–5850.